Quasiperiodic driving of Anderson localized waves in one dimension

H. Hatami,[1] C. Danieli,[2] J. D. Bodyfelt,[2] and S. Flach[1,2]

[1]*Center for Theoretical Physics of Complex Systems, Institute for Basic Science, Daejeon, Korea*

[2]*New Zealand Institute for Advanced Study, Centre for Theoretical Chemistry & Physics, Massey University, Auckland, New Zealand*

(Received 8 February 2016; published 9 June 2016)

We consider a quantum particle in a one-dimensional disordered lattice with Anderson localization in the presence of multifrequency perturbations of the onsite energies. Using the Floquet representation, we transform the eigenvalue problem into a Wannier-Stark basis. Each frequency component contributes either to a single channel or a multichannel connectivity along the lattice, depending on the control parameters. The single-channel regime is essentially equivalent to the undriven case. The multichannel driving increases substantially the localization length for slow driving, showing two different scaling regimes of weak and strong driving, yet the localization length stays finite for a finite number of frequency components.

DOI: 10.1103/PhysRevE.93.062205

I. INTRODUCTION

Disordered systems have attracted a great deal of interest for transport phenomena since Anderson predicted that waves localize in the presence of uncorrelated random potentials [1]. By obtaining the exponential decay of every eigenstate of a disordered class of one-dimensional linear wave equations, Anderson proved the localization of a single quantum particle, within a finite volume of the chain, due to disorder. Ever since then, theoretical studies have been performed on higher-dimensional lattices in random potentials, showing the absence of diffusion in the two-dimensional case [2], and mobility edges between the insulating and the metallic phase in the three-dimensional case [3]. In one dimension, Anderson localization has been observed in experiments with light waves [4] and atomic Bose-Einstein condensates [5,6], enhancing further interest in theoretical research of disordered systems.

Wave localization inherently relies on the phase coherence within the wave state. If the disordered potential is allowed to temporarily fluctuate in a random way, phase coherence is lost, and the previously localized wave starts to diffuse without limits [7,8]. Assuming that the temporal fluctuations are represented as a quasiperiodic function of time with D incommensurate fundamental frequencies, the random noise can be effectively reached in the limit of $D \to \infty$. Here we address the case of a finite number of frequencies (colors) D. Will the localization length ζ stay finite for any finite D? If yes, what is its dependence on D? At fixed D, how does ζ depend on the remaining control parameters, such as frequency, fluctuation amplitude, and disorder strength?

A series of computational studies was devoted to this very issue [9–11]. While the first conclusion was that Anderson localization can be destroyed for $D \geqslant 2$, a more accurate recomputation showed that the localization length might well increase, yet stay finite. Other studies considered the case of single-color $D = 1$ homogeneous external ac fields [12–14]. In particular, Martinez *et al.* [12] reported on numerical evidence of the localization length increase with decreasing driving frequency, while Refs. [13,14] focused on the properties of conductance statistics in finite samples.

In this work, we first consider a single frequency color, that is, a time-periodic drive. We use the Floquet representation to arrive at a time-independent eigenvalue problem on a two-dimensional lattice, with one direction corresponding to the original spatial extension, and the second one to the Floquet (driving) one. We transform into a Wannier-Stark basis that is diagonal along the Floquet direction, and we analyze the resulting eigenvalue problem. For large driving frequencies, the equations reduce to uncoupled single-channel ones, which are essentially equivalent to the undriven case. For small driving frequencies, we obtain a multichannel regime with a substantial increase of the localization length and its divergence in the limit of vanishing frequency. This multichannel regime divides into two further regimes of weak and strong driving amplitudes, which yield different scaling laws. We then generalize to the case of many incommensurate frequencies, and we compare our findings to numerical results.

The paper is organized as following. In Sec. II, we introduce the model and its general features. In Sec. III, we derive the results for one frequency (color) drive. We generalize to many colors in Sec. IV, and we discuss numerical results in Sec. V. We conclude with discussions, a summary, and an outlook.

II. MODEL

We consider a disordered one-dimensional tight-binding chain in the presence of a coherent time-dependent driving of the onsite energies. The equations of motion read

$$i\dot{\psi}_l = \epsilon_l \left[1 + \sum_{i=1}^{D} \mu_i \cos(\omega_i t + \phi_l^i)\right] \psi_l - \lambda(\psi_{l+1} + \psi_{l-1}). \tag{1}$$

The onsite energies of each lattice site ϵ_l are random uncorrelated numbers with a probability density function (PDF) of value $1/W$ inside the interval $\epsilon_l \in [-W/2, +W/2]$ and zero outside. The parameter W parametrizes the strength of the disorder. The coefficient λ is the strength of the hopping between nearest-neighbor lattice sites, while μ_i and ω_i, respectively, are the amplitude and frequency of the ith driving. D is the total number of frequencies (colors) in the driving. The frequencies $\Omega = (\omega_1, \ldots, \omega_D)$ are chosen incommensurate with each other,

$$\mathbf{k} \cdot \Omega = k_1\omega_1 + \cdots + k_D\omega_D \neq 0, \quad \forall\, \mathbf{k} \in \mathbb{Z}^D \setminus \{0\}. \tag{2}$$

The random phases ϕ_l are uncorrelated and have a PDF of value $1/(2\pi)$ inside the irreducible interval $\phi_l \in [-\pi,\pi]$. Their presence ensures broken time-reversal symmetry of (1). For $\mu_i = 0$, Eq. (1) reduces to the well-known Anderson model with all eigenstates being localized with a finite upper bound on the localization length [1,15].

The above model can be realized experimentally in atomic Bose-Einstein condensates when laser beams with different frequencies perturb the atomic system and also the optical lattice itself [16,17]. Similar models have been considered for the conductivity of electrons in two-dimensional confinements with local scatterers (defects, phonons) acting as time-dependent sources of dephasing [8]. Other approaches consider noise in external ac fields, which should not change the physics outcome dramatically [12–14].

III. ONE COLOR

We first consider a driving with only one frequency $D = 1$. In this case, Eq. (1) reads

$$i\dot{\psi}_l = \epsilon_l[1 + \mu\cos(\omega t + \phi_l)]\psi_l - \lambda(\psi_{l+1} + \psi_{l-1}). \quad (3)$$

Since the perturbation is time-periodic with period $T = \frac{2\pi}{\omega}$, we first perform a Floquet expansion that will yield an effective two-dimensional lattice problem.

A. From Floquet to Wannier-Stark

According to the Floquet theorem [18,19], a solution of (3) is given by

$$\psi_l(t) = u_l(t)e^{-iEt}, \quad (4)$$

where E is the quasienergy and the Floquet functions $u_l(t) = u_l(t+T)$. They can be represented in a Fourier series

$$u_l(t) = \sum_k A_{l,k}e^{ik(\omega t+\phi_l)}. \quad (5)$$

The Floquet expansion of the wave function $\psi_l(t)$ is then given by

$$\psi_l(t) = \sum_k A_{l,k}e^{-i[(E-k\omega)t-k\phi_l]}. \quad (6)$$

This transformation maps Eq. (3) into a time-independent eigenvalue problem on a two-dimensional lattice (see the Appendix),

$$EA_{l,k} = (\epsilon_l + k\omega)A_{l,k} + \frac{\mu\epsilon_l}{2}(A_{l,k-1} + A_{l,k+1}) - \lambda(\xi^-_{l,k}A_{l-1,k} + \xi^+_{l,k}A_{l+1,k}) \quad (7)$$

with the coefficients

$$\xi^\pm_{l,k} = e^{-ik(\phi_l-\phi_{l\pm1})} = e^{-ik\theta^\pm_l} \quad (8)$$

dependent on the random phase differences $\theta^\pm_l = \phi_l - \phi_{l\pm1}$, which introduce a synthetic gauge field in the two-dimensional lattice of Eq. (7)

Consider first $\lambda = 0$. We can solve the remaining eigenvalue problem for each lattice site l independently, as this case corresponds to the well-known Wannier-Stark ladder [20] under an effective dc electric field ω- and l-dependent hopping coefficient $\mu\epsilon_l/2$. The eigenfunctions $B^{(\nu)}_{l,k} = J_{k-\nu}(\mu\epsilon_l/\omega)$ are obtained using the Bessel function of the first kind, $J_k(x)$, with fixed argument x, and their eigenvalues form equidistant spectra $E_{\nu,l} = \epsilon_l + \omega\nu$ [22,23]. These eigenfunctions are localized (along the Fourier direction k), with tails that decay superexponentially fast. The localization volume (size) $\mathcal{L}$ of an eigenstate is estimated as $\mathcal{L} \sim 2|\frac{\mu\epsilon_l}{\omega}|$ for $\frac{\omega}{\mu\epsilon_l} \leqslant 10$, and it reaches its asymptotic value $\mathcal{L} = 1$ for $\frac{\omega}{\mu\epsilon_l} \geqslant 10$ [21].

We use these Wannier-Stark eigenstates as a new basis for each lattice site l of (7):

$$A_{l,k} = \sum_\nu c_{l,\nu}B^{(\nu)}_{l,k}. \quad (9)$$

The transformed eigenvalue problem for $\lambda \neq 0$ reads (see the Appendix)

$$Ec_{l,\nu} = (\epsilon_l + \omega\nu)c_{l,\nu} - \lambda\sum_s[e^{is\varphi^-_l}J_s(\Delta^-_l)c_{l-1,\nu-s} + e^{is\varphi^+_l}J_s(\Delta^+_l)c_{l+1,\nu-s}], \quad (10)$$

where

$$\tan\varphi^\pm_l = -\frac{\epsilon_{l\pm1}\sin\theta^\pm_l}{\epsilon_l - \epsilon_{l\pm1}\cos\theta^\pm_l},$$
$$\Delta^\pm_l = \frac{\mu}{\omega}\sqrt{\epsilon_l^2 + \epsilon_{l\pm1}^2 - 2\epsilon_l\epsilon_{l\pm1}\cos\theta^\pm_l}. \quad (11)$$

This eigenvalue problem has zero hoppings along the Fourier direction ν. Instead, each lattice site $c_{l,\nu}$ is connected to a number of nearest-neighbor sites $c_{l\pm1,\nu-s}$ given by the complex hopping coefficients $e^{is\phi^\pm_l}J_s(\Delta^\pm_l)$ (see Fig. 1). The number of strong links (connectivity) with a given site at l,ν depends on the ratio of the difference in the new onsite energies $|\epsilon_l - \epsilon_{l\pm1} + s\omega|$ and the hopping strength $|J_s(\Delta^\pm_l)|$. Strong links are then characterized by $|(\epsilon_l - \epsilon_{l\pm1} + s\omega)/J_s(\Delta^\pm_l)| \leqslant 1$.

B. Single-channel versus multichannel regimes

In the case of zero driving strength, $\mu = 0$, it follows that $\Delta^\pm_l = 0$ for all l, and $J_s(0) = \delta_{s,0}$. The two-dimensional lattice Eq. (10) turns into an infinite set of independent one-dimensional Anderson chains. For nonzero driving strength ($\mu \neq 0$), all the Floquet channels are connected. Since [22,23]

$$J_s(\Delta^\pm_l) \longmapsto \frac{(\Delta^\pm_l)^s}{2^s s!} \quad \text{for } s \longmapsto +\infty, \quad (12)$$

only a finite number of channels will have a nonexponentially weak hopping strength, and that number depends on the value of the argument of the Bessel functions $\Delta^\pm_l$. If for every l the argument is close to zero, $|\Delta^\pm_l| \leqslant \delta \ll 1$, it follows that $J_0(\Delta^\pm_l) \approx 1$, and for $s \neq 0$ the Bessel functions $J_s(\Delta^\pm_l)$ decay as Eq. (12). As a consequence, Eq. (10) becomes an infinite set of uncoupled equivalent Anderson chains, and the model resembles the unperturbed case. We call this the *single-channel regime*. This result is true irrespective of the ratio of ω/W, which controls the energy differences between connected sites. While this is evident for large frequencies $\omega \gg W$ (where the energy difference is of order W), it is also true in the opposite limit $\omega \ll W$ where the energy difference can be of order ω for

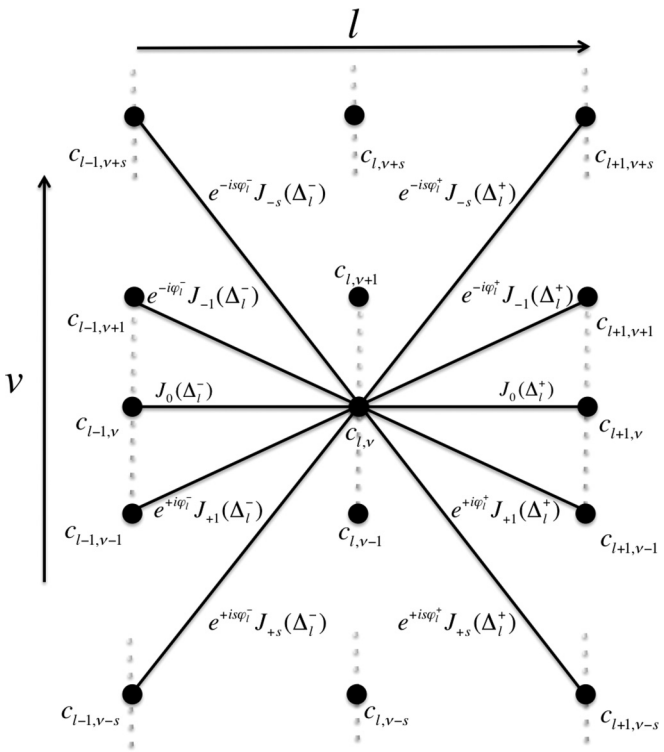

FIG. 1. Two-dimensional eigenvalue problem Eq. (10). Each given site (l,ν) is connected to a set of sites $(l\pm1,\nu-s)$ through the hopping $e^{is\phi_l^\pm}J_s(\Delta_l^\pm)$.

a suitably large value of $s\sim W/\omega$, since the hoppings decay superexponentially fast with large s (12).

In contrast, when $\Delta_l^\pm\geqslant 1$, a finite number $\mathcal{L}_l^\pm$ of the Bessel functions $J_s(\Delta_l^\pm)$ for $s\neq 0$ are not negligible. Their typical values can be approximated as [22,23]

$$J_s(\Delta_l^\pm)\approx\sqrt{\frac{2}{\pi\Delta_l^\pm}}\cos\left(\Delta_l^\pm-\frac{s\pi}{2}-\frac{\pi}{4}\right),\quad |s|\leqslant\frac{\mathcal{L}_l^\pm}{2}. \tag{13}$$

In Eq. (11), the square root of $\Delta_l^\pm$ is on the order of the disorder strength W. We define the parameter Δ as

$$\Delta_l^\pm\quad\longmapsto\quad\Delta=\frac{\mu W}{\omega}. \tag{14}$$

It follows that, if $\Delta\geqslant 1$, the averaged number of connected channels $\mathcal{L}$ is given by

$$\mathcal{L}_l^\pm=2\Delta_l^\pm\quad\longmapsto\quad\mathcal{L}=2\Delta=\frac{2\mu W}{\omega}, \tag{15}$$

while in Eq. (13), neglecting the cosine term that represents the Bessel function oscillation, the general value of the hopping can be approximated as

$$J_s\approx\sqrt{\frac{2}{\pi\Delta}}=\sqrt{\frac{2\omega}{\pi\mu W}},\quad |s|\leqslant\frac{\mathcal{L}}{2}. \tag{16}$$

We call this regime the *multichannel regime*. Therefore, for any given disorder and driving strengths W and μ, this regime will be realized in the limit of small frequencies ω. This latter regime will be the focus of our investigation, since in the single-channel regime the model acts similar to the undriven case. Our results confirm earlier intuitive interpretations that the increase in the channel number can be responsible for a substantial increase in the localization length in the presence of adiabatic single-color external ac driving [12,13].

C. The multichannel regime

1. Weak driving

Let us first consider the case $\mu\ll 1$. For a given site (l,ν) there are $\mathcal{L}$ matrix elements connecting this site to a set of sites $(l+1,\nu')$. The onsite energies of these connected sites vary in an interval $[\epsilon_{l+1}-\mu W,\epsilon_{l+1}+\mu W]$. For $\mu\ll 1$ this interval is narrow compared to W, which characterizes the spread of ϵ_l. Therefore, the difference in the onsite energies between two connected sites is still of the order W.

In general, for ladders with a finite number N of equivalent Anderson chains, Dorokhov, Mello, Pereyra, and Kumar [24,25] estimate the localization length ζ of an N-leg ladder as a product of the localization length $\zeta_{\mathcal{A}}$ of each leg and the number of legs N:

$$\zeta\sim N\zeta_{\mathcal{A}}. \tag{17}$$

The number of legs N corresponds to $\mathcal{L}$. The single-channel localization length can be estimated using the ratio W_{eff} between the energy mismatch (disorder strength) W and the matrix element λJ_s from (16):

$$W_{\text{eff}}=\frac{W^{\frac{3}{2}}}{\lambda}\sqrt{\frac{\mu\pi}{2\omega}}. \tag{18}$$

We then obtain [15]

$$\zeta_{\mathcal{A}}(\omega)\sim\begin{cases}\frac{100}{W_{\text{eff}}^2} & \text{if}\quad W_{\text{eff}}\leqslant 10,\\ \frac{1}{|\ln(1/W_{\text{eff}})|} & \text{if}\quad W_{\text{eff}}>10.\end{cases} \tag{19}$$

It follows that in the case of weak effective disorder, $W_{\text{eff}}\leqslant 10$, the localization length ζ of our driven model is given by

$$\zeta(\omega)\sim\frac{400\lambda^2}{\pi W^2},\quad\omega\geqslant\frac{\mu\pi W^3}{200\lambda^2}. \tag{20}$$

The localization length ζ does not depend on the frequency ω and the driving strength μ, since the increase of the number of connections $\mathcal{L}$ and the decrease of the localization length $\zeta_{\mathcal{A}}$ along each Anderson chain balance each other. Upon further decrease of the frequency ω, this balancing effect is destroyed since Δ grows, the matrix element λJ_s decays, and the effective disorder $W_{\text{eff}}>10$. With (19) it follows that

$$\zeta(\omega)=\frac{2\mu W}{\omega}\left|\ln\left(\frac{\lambda}{W^{\frac{3}{2}}}\sqrt{\frac{2}{\pi\mu}\omega}\right)\right|^{-1},\quad\omega\leqslant\frac{\mu\pi W^3}{200\lambda^2}. \tag{21}$$

The localization length then diverges for $\omega\to 0$.

To summarize: in the weakly driven multichannel regime we expect a plateau in the dependence $\zeta(\omega)$ for $\omega\geqslant\frac{\mu\pi W^3}{200\lambda^2}$, which is replaced by a divergence for $\omega\leqslant\frac{\mu\pi W^3}{200\lambda^2}$.

2. Strong driving

Let us consider the case $\mu\geqslant 1$, and constant phases $\phi_l=\text{const}$. For a given site (l,ν) there are $\mathcal{L}$ matrix elements connecting this site to a set of sites $(l+1,\nu')$. The onsite energies of these connected sites vary in an interval $[\epsilon_{l+1}-$

$\mu W, \epsilon_{l+1} + \mu W]$. For $\mu \geqslant 1$ this interval is larger than W, which characterizes the spread of ϵ_l. Therefore, there will be typically one onsite energy among the connected set, which is detuned by a mismatch of order ω from the one onsite (l, ν). It follows that for $\mu \geqslant 1$ and $\omega \ll W$ we can trace a path in Eq. (10) where the onsite mismatch is of the order of the frequency $|\epsilon_l - \epsilon_{l\pm1} + s\omega| \sim \omega$ and the hopping scales with the square root of the frequency $J_s \sim \sqrt{\omega}$ for every l. We call this the *optimal path*. The optimal path is a one-dimensional random walk within the two-dimensional network. Along that optimal path, the localization length ζ_{opt} follows from the effective disorder W_{eff} between the energy mismatch (disorder strength) ω and the matrix element λJ_s from (16),

$$\zeta_{\text{opt}}(\omega) = \frac{100 J_s^2}{\omega^2} = \frac{100}{\omega^2}\left(\sqrt{\frac{2\omega}{\pi \mu W}}\right)^2 = \frac{200}{\pi \mu W}\frac{1}{\omega}. \quad (22)$$

For small frequencies, this optimal path consists of strong links. Furthermore, paths neighboring the optimal one are also strong links, as long as the energy detuning does not exceed the matrix element. Since the matrix element scales with $\sqrt{\omega}$, the number of strong links diverges as $N \sim 1/\sqrt{\omega}$. Using the Dorokhov estimates, we conclude that the localization length on the network is scaling as

$$\zeta \sim \frac{200}{\pi \mu W}\frac{1}{\omega^{3/2}}. \quad (23)$$

Therefore, the localization length diverges for vanishing frequency faster than in the weak driving case.

3. *Local suppression of strong driving*

The presence of random phases will suppress the optimal path through an increase of the minimal value of the driving strength:

$$\mu\sqrt{1 + \frac{2\epsilon_l \epsilon_{l\pm1}}{(\epsilon_l - \epsilon_{l\pm1})^2}(1 - \cos\theta_l^{\pm})} \geqslant 1, \quad (24)$$

where $\theta_l^{\pm} = \phi_l - \phi_{l\pm1}$. In particular, if $\theta_l^{\pm} = \pi$, the square root term of Eq. (24) is equal to zero if

$$-2\epsilon_l \epsilon_{l\pm1} = \epsilon_l^2 + \epsilon_{l\pm1}^2 \quad \Leftrightarrow \quad \epsilon_l = -\epsilon_{l\pm1}. \quad (25)$$

In this case, Eq. (24) does not hold for any finite value of μ, and locally between site l and site $l \pm 1$ the optimal path is not accessible.

Therefore, for uncorrelated phases ϕ_l, the square root term of Eq. (24) can be arbitrarily close to zero if $\theta_l^{\pm} \approx \pi$ and $\epsilon_l \approx -\epsilon_{l\pm1}$. As a consequence, μ has to diverge to infinity in order to satisfy Eq. (24) at every step l, and so, for given finite values of the driving strength, the optimal path is interrupted. This will lead to a slower divergence of the localization length, which, however, is still expected to be faster than in the weak driving regime, since there will be finite volume parts in which the optimal path will survive.

4. *Local suppression of the multichannel regime*

Since ϵ_l and ϕ_l are random phases, the square root term of Eq. (11) can be arbitrarily close to zero. Therefore, even deep in the multichannel regime $\Delta \gg 1$, there might exist one or more lattice sites l such that the Bessel function argument $\Delta_l^{\pm} \ll 1$. In that case, the hopping $J_s(\Delta_l^{\pm}) \approx \delta_{s,0}$ as in the single-channel regime. As a result, the multichannel regime between sites l and $l \pm 1$ becomes locally suppressed.

In the case of constant phases $\phi_l = \text{const}$, this local suppression appears if $|\epsilon_l - \epsilon_{l\pm1}| \ll \omega/\mu$. The single channel then still shows an energy difference of the order of ω or less, similar to the optimal path. For uncorrelated phases ϕ_l, the probability of a local suppression of the multichannel regime is reduced. Indeed, in order to violate the multichannel condition $\Delta_l^{\pm} \gg 1$, we now need to request either $|\epsilon_l - \epsilon_{l+1}| \ll \omega^2/\mu^2$ and $|\theta_l^{\pm}| \ll 1$ or $|\epsilon_l + \epsilon_{l+1}| \ll \omega^2/\mu^2$ and $||\theta_l^{\pm}| - \pi| \ll 1$. The previously obtained estimates on the localization length ζ in either weak and strong driving regimes are therefore upper bounds.

IV. MANY COLORS

For the general case of Eq. (1), the Floquet expansion in momentum space and the rotation of the eigenvalue problem in a basis of Bessel functions for each frequency are a natural generalization of what we have previously described in Sec. III for one color $D = 1$ (see the Appendix). Since the frequency components of Ω are chosen to be incommensurate [Eq. (2)], the general form of the Floquet expansion (6) runs over the vector index $\mathbf{k} = (k_1, \ldots, k_D) \in \mathbb{Z}^D$ [26], and it yields a $(D+1)$-dimensional time-independent eigenvalue problem:

$$E c_{l,\mathbf{v}} = (\epsilon_l + \Omega \cdot \mathbf{v}) c_{l,\mathbf{v}} - \lambda \sum_{\mathbf{s}} [e^{i\mathbf{s}\cdot\Phi_l^-} \mathcal{J}_{\mathbf{s}}^- c_{l-1,\mathbf{v}-\mathbf{s}} + e^{i\mathbf{s}\cdot\Phi_l^+} \mathcal{J}_{\mathbf{s}}^+ c_{l+1,\mathbf{v}-\mathbf{s}}], \quad (26)$$

where $\mathbf{s}, \mathbf{v} \in \mathbb{Z}^D$ and $\Phi_l^{\pm} = (\varphi_{l,i}^{\pm})_{i=1}^D$. The coefficients are defined as

$$\tan\varphi_{l,i}^{\pm} = -\frac{\epsilon_{l\pm1}\sin\theta_{l,i}^{\pm}}{\epsilon_l - \epsilon_{l\pm1}\cos\theta_{l,i}^{\pm}},$$
$$\mathcal{J}_{\mathbf{s}}^{\pm} = \prod_{i=1}^{D} J_{s_i}(\Delta_{l,i}^{\pm}), \quad (27)$$
$$\Delta_{l,i}^{\pm} = \frac{\mu_i}{\omega_i}\sqrt{\epsilon_l^2 + \epsilon_{l\pm1}^2 - 2\epsilon_l\epsilon_{l\pm1}\cos\theta_{l,i}^{\pm}},$$

which depend on the random phase difference $\theta_{l,i}^{\pm} = \phi_l^i - \phi_{l\pm1}^i$ for $i = 1, \ldots, D$. The resulting eigenvalue problem Eq. (26) has D frequency (color) directions (with zero hopping along them), and each site $c_{l,\mathbf{v}}$ is connected to the nearest-neighbor ones $c_{l\pm1,\mathbf{v}-\mathbf{s}}$ through the complex matrix elements $e^{i\mathbf{s}\cdot\Phi_l^{\pm}}\mathcal{J}_{\mathbf{s}}^{\pm}$. Each frequency color will add to the total number of channels.

Let us assume that all frequency components satisfy the same condition for single or multichannel (either strong or weak driving) regimes. Then we conclude that the single-channel regime will be applicable to multicolor driving as well, i.e., in the limit of large frequencies, localization length corresponds to its value from the undriven case. In the multichannel regime, using the above argument of Dorokhov, the localization length ζ_D will be of the order of $\zeta_D \sim D\zeta$, with ζ being the corresponding single-color localization length discussed in the previous section. Therefore, the localization

length will stay finite for any finite number of colors. The divergence of ζ_D in the limit of $D \to \infty$ is in agreement with the result that random noise driving leads to dephasing and complete delocalization [7,8].

V. NUMERICAL RESULTS

We first analyze the single-color driving and then discuss the two-color case. We decide not to diagonalize the eigenvalue problem Eq. (7), since this will limit the required system size N and the number of colors D. Instead, we compute the spreading of the wave packet over time for a single site excitation $\psi_l(t=0) = \delta_{l,N/2}$ as an initial condition using a numerical symplectic integration scheme $SBAB_2$ [27,28]. This method keeps the norm fluctuations bounded, and it allows us to easily incorporate any number of colors without significant additional computational expense. However, the number of colors increases the expected localization length, and therefore there will be an overall restriction on the number of colors that can be implemented in a computational run with a CPU time of the order of one week.

To measure the evolution of the wave packet, we calculate the second moment m_2, which, for localized modes, estimates the squared distance between the eigenmode tails. It is related to the localization length ζ of one mode as $m_2 \sim \zeta^2$, and it is defined as

$$m_2(t) = \sum_l \left(l - \sum_{l'} l' |\psi_{l'}(t)|^2 \right)^2 |\psi_l(t)|^2. \qquad (28)$$

Hereafter, unless indicated differently, in Eq. (1) we choose the hopping amplitude $\lambda = 1$ and the disorder strength $W = 4$. Furthermore, for the numerical computations we choose a system size $N = 1024$ and we average $\log_{10} m_2(t)$ over 512 disorder realizations, unless stated otherwise.

A. One color

Let us analyze the frequency dependence of the time evolution. For the *weak driving* case we choose the driving strength $\mu = 0.1$. The multichannel regime ($\Delta \geqslant 1$) is then obtained for frequencies $\omega \leqslant 0.4$. The time evolution of the second moment m_2 is shown in Fig. 2.

We observe that the second moment first increases with time but saturates at later times, indicating a halt of spreading and a localization of the wave packet. Therefore, we conclude that there is a finite upper bound on the localization length ζ of the corresponding eigenvalue problem. The onset of spreading beyond the undriven reference curve (black curve in Fig. 2) scales inversely with the driving frequency, as expected.

We use the saturated value of the second moment at time $t = 10^6$ as a measure of the squared localization length, and we plot it as a function of frequency ω in Fig. 3. Increasing ω in the single-channel regime $\omega > 0.4$ leads to a quick decay of the saturated second moment to reach the reference value of the undriven case already at $\omega \approx 4$. In the multichannel regime, we observe two features: a plateau at an intermediate frequency interval, and a subsequent increase of the saturated second moment by further lowering the frequency. This is in agreement with our analytics in Sec. III C 1.

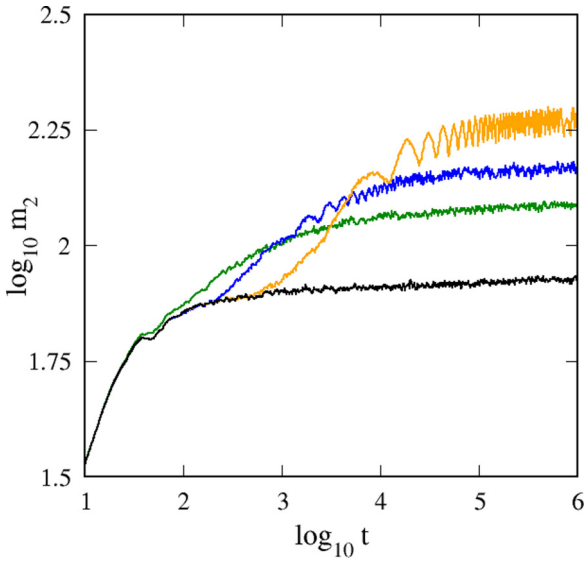

FIG. 2. Time evolution of the second moment m_2 with driving strength $\mu = 0.1$. Frequency values (from top to bottom at the right edge of the plot): $\omega = 5 \times 10^{-4}$ (orange), $\omega = 5 \times 10^{-3}$ (blue), $\omega = 10^{-1}$ (green), and undriven (black).

For the *strong driving* regime, we consider a driving strength $\mu = 1$. In Fig. 4 we plot the time evolution of the second moment m_2 for different frequencies in the multichannel regime $\omega \leqslant 5$. The second moment m_2 increases as the frequency ω decreases, in agreement with Eq. (23). Moreover, we observe the appearance of transient regions of normal diffusion that extend their length as the frequency ω decreases. Again, $m_2(t)$ saturates at larger time, indicating a halt of spreading and a localization of the wave packet. The frequency dependence of the saturated values of the second moment m_2 is shown in Fig. 5, where we plot the second moment of the wave packet at time $t = 10^5$ as function of the

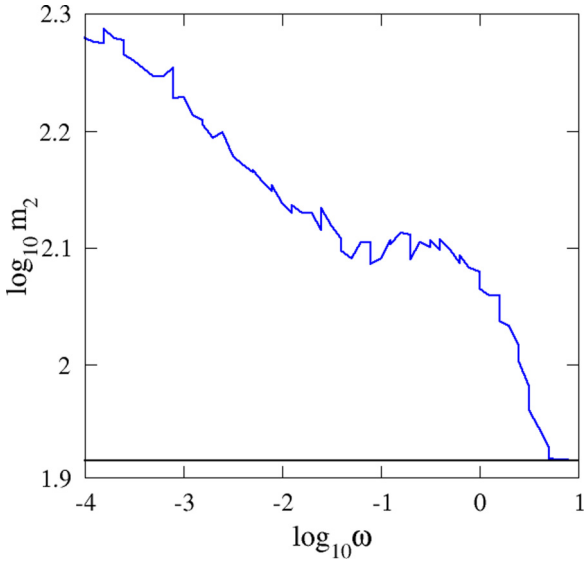

FIG. 3. Saturated second moment m_2 at $t = 10^6$ as a function of frequency ω of a one-color perturbation with $\mu = 0.1$. The black horizontal line indicates the value for the undriven case.

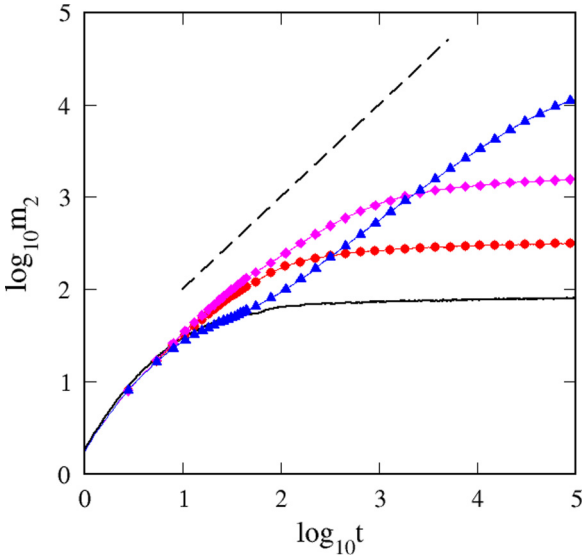

FIG. 4. Time evolution of the second moment m_2 with driving strength $\mu = 1$. The dashed line indicates normal diffusion $m_2 \sim t$. Frequency values: $\omega = 5$ (black), $\omega = 2$ (red circles), $\omega = 0.5$ (magenta diamonds), and $\omega = 0.02$ (blue triangles).

frequency ω. For comparison, we also replot the weak driving curve from Fig. 3.

Similar to the weak driving (blue curve), the second moment for the strong driving (red curve) tends to the undriven case (black horizontal line) for large frequencies and diverges for small ones. In agreement with Eq. (23), the plateau (which was observed for weak driving) is suppressed, although a reminding shoulder exists at $\omega \approx 2.5$. The strong driving yields much larger values of the saturated second moment as compared to the weak driving case, in accord with our predictions. The frequency dependence is weaker than the

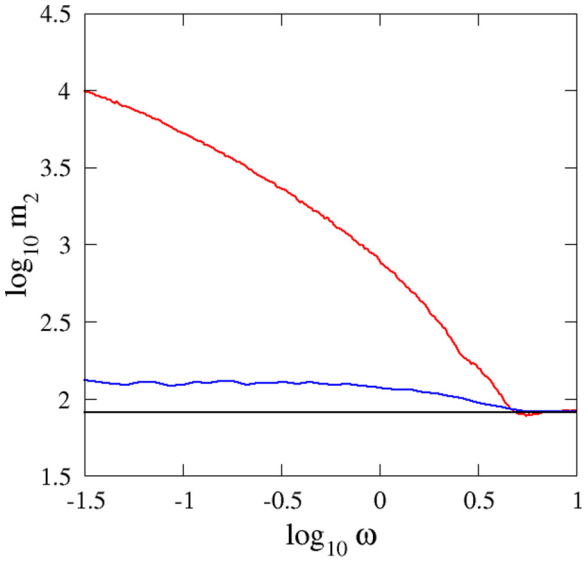

FIG. 5. Saturated second moment m_2 at $t = 10^5$ as a function of frequency ω of a one-color perturbation with $\mu = 0.1$ (blue, bottom) and $\mu = 1$ (red, top). The black horizontal line indicates the value of the undriven case.

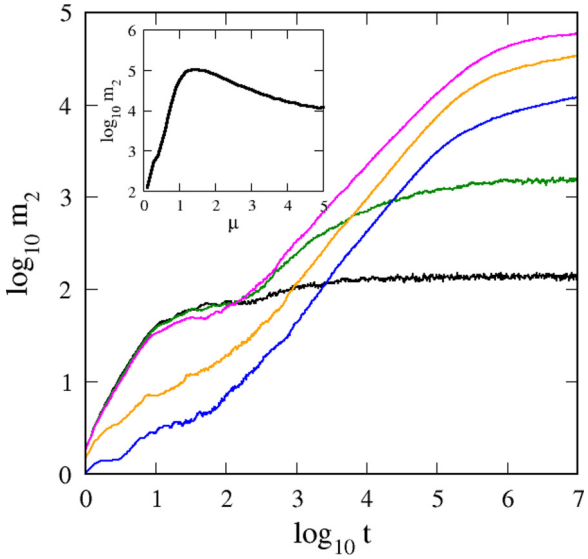

FIG. 6. Time evolution of the second moment m_2 with frequency $\omega = 5 \times 10^{-3}$. Driving strength values (from top to bottom at the right edge of the plot): $\mu = 1.0$ (magenta), $\mu = 3.0$ (orange), $\mu = 5.0$ (blue), $\mu = 0.5$ (green), and $\mu = 0.1$ (black). The inset shows the dependency of the almost saturated second moment m_2 at $t = 10^7$ on the drive strength. System size $N = 2048$, and $\log_{10} m_2$ is averaged over 32 disorder realizations.

predicted law in Eq. (23), most likely due to the discussed local suppression of strong driving and multichannel regimes.

In Fig. 6 we plot the time evolution of the second moment m_2 for different values of the driving strength μ in the strong driving regime. The inset of Fig. 6 shows the dependence of the almost saturated second moment m_2 at $t = 10^7$ on μ. We observe that the saturated moment increases up to $\mu \approx 1$ and starts to decrease for larger values of μ. This subsequent decrease is in qualitative agreement with the prediction $\zeta \sim \frac{1}{\mu}$ following from Eq. (10). We also note that the data for large values of μ did not completely saturate, due to limitations in the computational power.

We note that Nakanishi *et al.* [8] have studied the dynamics of a quantum particle (electron) in a two-dimensional setting with a single-color strong driving in the adiabatic regime of small frequencies. There an unbounded normal diffusion was reported, which is probably due to the higher dimensionality of the underlying lattice. We further mention the numerical study of the increase of the localization length with decreasing frequency of an external ac field [12], which is similar to our analytical and numerical results for single-color fluctuating potentials.

B. Two colors

We assume the driving strengths to be equal, $\mu_1 = \mu_2$, and we fix the frequency relation $\omega_2 = \sqrt{2}\omega_1$. We first consider the *weak driving* case. In Fig. 7, we compare one- and two-color cases for the same driving strength $\mu = 0.1 = \mu_1$ and frequency $\omega = 3 \times 10^{-2} = \omega_1$.

The presence of a second incommensurate driving term enhances the spreading of the wave packet. However, the

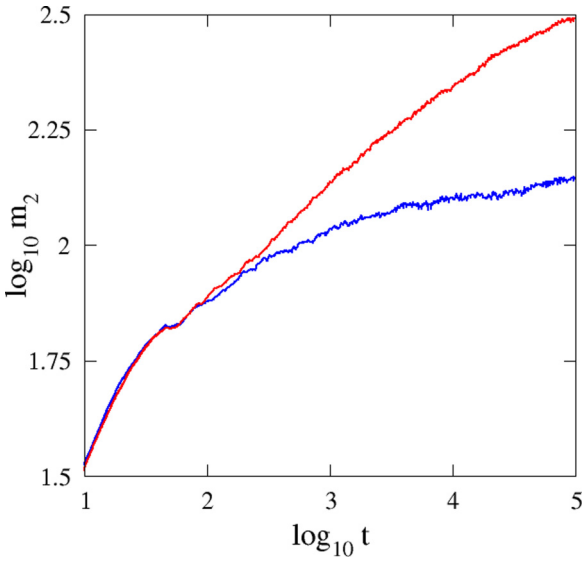

FIG. 7. Time evolution of the second moment m_2 for one-color (blue, bottom) and two-color (red, top) cases with driving strength $\mu = \mu_1 = 0.1$ and frequency $\omega = \omega_1 = 3 \times 10^{-2}$. We recall $\omega_2 = \sqrt{2}\omega_1$ for the two-color case.

integration time $t = 10^5$ is not enough to see the saturation of the second moment.

To obtain saturation at time $t = 10^5$, we reduce the driving strength to $\mu_1 = 0.05 = \mu_2$. In Fig. 8 we plot the saturated value of the second moment m_2 at time $t = 10^5$ as a function of the frequency ω_1, and we compare it to the weak driving single-color result ($\mu = 0.1$) from Fig. 3. The values approach the undriven case (black horizontal line) for approximately $\omega_1 \geqslant 4$, in good agreement with the single-channel regime $\omega_1, \omega_2 \geqslant 2$. Similar to the one-color case, the saturated second

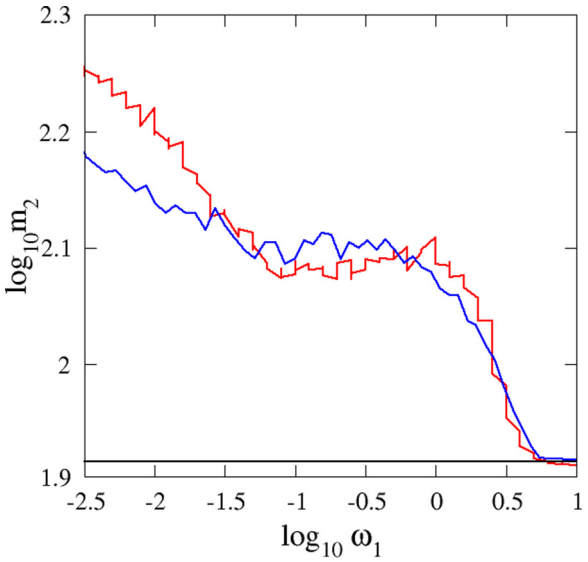

FIG. 8. Saturated second moment m_2 at $t = 10^5$ as a function of driving frequency ω_1 with driving strengths $\mu_1 = \mu_2 = 0.05$ (red curve, top left corner). The blue curve corresponds to the single color one from Fig. 3. We recall $\omega_2 = \sqrt{2}\omega_1$. The black horizontal line indicates the value of the undriven case.

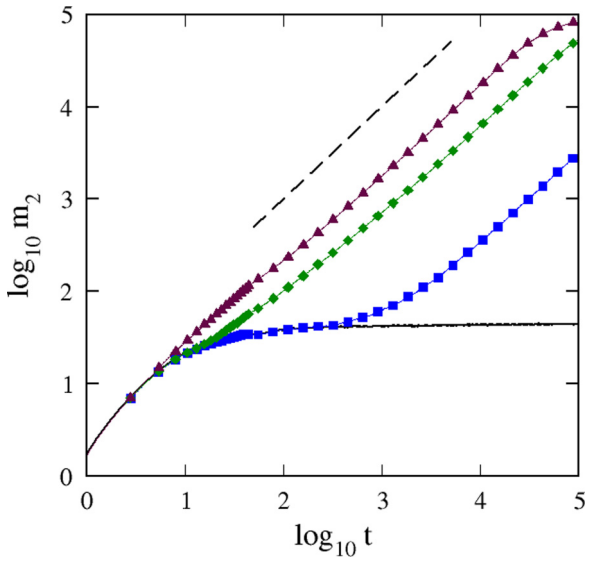

FIG. 9. Time evolution of the second moment m_2 with driving strength $\mu_1 = \mu_2 = 1$. We recall $\omega_2 = \sqrt{2}\omega_1$. The dashed line indicates normal diffusion $m_2 \sim t$. Frequency values: $\omega_1 = 5 \times 10^{-1}$ (maroon triangles), $\omega_1 = 5 \times 10^{-2}$ (green diamonds), $\omega_1 = 5 \times 10^{-4}$ (blue squares), undriven (black).

moment exhibits a plateau in the multichannel regime. Notably the height of the plateau is practically equal to the single-color one reported in Fig. 3, in full accord with our estimate of the localization length in Eq. (20), which is independent of the driving strength μ and more generally independent of the number of participating channels. Therefore, the presence of a second frequency that increases the number of channels should not change the plateau value, as observed.

For the *strong driving* case, we consider $\mu_1 = \mu_2 = 1$. In Fig. 9 we show the time evolution of the second moment m_2 for frequencies $\omega_{1,2}$ chosen in the multichannel regime. We observe long-lasting transient regions of diffusive spreading, with a clear tendency toward a subsequent halt and localization.

Again the onset of spreading beyond the undriven reference curve (black curve in Fig. 9) is scaling inversely with the driving frequency, as expected, similar to the $D = 1$ case. We also observe a significant increase in the localization length as compared to the single-color case, in agreement with our predictions.

VI. SUMMARY AND CONCLUSIONS

In this work, we have studied the spreading of a wave packet for a one-dimensional disordered chain in the presence of a multifrequency quasiperiodic drive. For each term (color) of the driving, the Floquet representation is used to arrive at a time-independent eigenvalue problem on a two-dimensional lattice, with one direction corresponding to the original spatial extension, and the second one to the Floquet (driving) one. We transform into a Wannier-Stark basis that is diagonal along the Floquet direction, and we analyze the resulting eigenvalue problem. For large driving frequencies the equations reduce to uncoupled single channel ones, which are essentially equivalent to the undriven case. For small driving frequencies,

we obtain a multichannel regime with a substantial increase of the localization length, and its divergence in the limit of vanishing frequency. This multichannel regime divides into two further regimes of weak and strong driving amplitudes, which yield different scaling laws.

In the many-colors case, we have shown that each incommensurate color is independent from the others and can be treated separately. The localization length of the model will then be proportional to the single-color localization length, and scales with the number of colors set in the multichannel regime. Therefore, it will remain finite for any finite number of colors.

Numerically, we have observed that in the strong driving, the model exhibits transient regions of diffusive dynamics before localization occurs. The localization volume increases as the number of colors increases when satisfying the multichannel regime condition. It follows that for $D \to \infty$, the localization length will diverge to infinity and the region of diffusive dynamics will extend to infinity until a complete delocalization is observed. The divergence of the number of colors D corresponds to the loss of quasiperiodicity of the driving term, and consequently to an effective random driving, which leads to a loss of Anderson localization in that limit.

Mathematical studies of the single color $D = 1$ case [29] and multicolor case $D > 1$ [30] predict stability of Anderson localization in the regime of strong disorder. These results are in line with our findings, since the limit of strong disorder corresponds to the single-channel regime, which is essentially independent of the number of colors, with a localization length close to that of the undriven case.

APPENDIX: FLOQUET ANALYSIS AND COORDINATE TRANSFORMATION

We focus on the one-color case $D = 1$ using Refs. [22,23]. The D color case is a generalization of these calculations. The one-dimensional time-dependent model Eq. (3) is mapped to a time-independent two-dimensional eigenvalue problem Eq. (7) via the Floquet expansion Eq. (4),

$$\psi_l(t) = \sum_k A_{l,k} e^{-i[(E-k\omega)t - k\phi_l]}. \tag{A1}$$

With

$$\begin{aligned}&\mu\epsilon_l \cos(\omega t + \phi_l)\psi_l \\ &\quad = \frac{\mu\epsilon_l}{2} \sum_k [A_{l,k-1} + A_{l,k+1}] e^{-i[(E-k\omega)t - k\phi_l]}\end{aligned} \tag{A2}$$

and

$$\begin{aligned}&\lambda(\psi_{l+1} + \psi_{l-1}) \\ &\quad = \lambda \sum_k [A_{l-1,k} e^{-i[(E-k\omega)t - k\phi_{l-1}]} \\ &\qquad + A_{l-1,k} e^{-i[(E-k\omega)t - k\phi_{l-1}]}] \\ &\qquad - \lambda \sum_k [A_{l-1,k} e^{-ik(\phi_l - \phi_{l-1})} e^{-i[(E-k\omega)t - k\phi_l]} \\ &\qquad + A_{l+1,k} e^{-ik(\phi_l - \phi_{l+1})} e^{-i[(E-k\omega)t - k\phi_l]}]\end{aligned} \tag{A3}$$

we define the hopping coefficients $\xi^{\pm}_{l,k}$ as

$$\xi^{\pm}_{l,k} = e^{-ik(\phi_l - \phi_{l\pm1})} \tag{A4}$$

to arrive at

$$\begin{aligned}&\sum_k (E - k\omega) A_{l,k} e^{-i[(E-k\omega)t - k\phi_l]} \\ &\quad = \sum_k \Big[\epsilon_l A_{l,k} + \frac{\mu\epsilon_l}{2}(A_{l,k-1} + A_{l,k+1}) \\ &\qquad - \lambda(\xi^-_{l,k} A_{l-1,k} + \xi^+_{l,k} A_{l+1,k}) \Big] e^{-i[(E-k\omega)t - k\phi_l]},\end{aligned} \tag{A5}$$

which finally yields the two-dimensional eigenvalue problem of Eq. (7),

$$\begin{aligned}E A_{l,k} &= (\epsilon_l + k\omega) A_{l,k} - \lambda(\xi^-_{l,k} A_{l-1,k} + \xi^+_{l,k} A_{l+1,k}) \\ &\quad + \frac{\mu\epsilon_l}{2}(A_{l,k-1} + A_{l,k+1}).\end{aligned} \tag{A6}$$

This is then transformed using Eq. (6):

$$A_{l,k} = \sum_\nu c_{l,\nu} B^{(\nu)}_{l,k}, \quad B^{(\nu)}_{l,k} = J_{k-\nu}\left(\frac{\mu\epsilon_l}{\omega}\right). \tag{A7}$$

The basis $\mathcal{B} = \{B^{(\nu)}_{l,k}\}_\nu$ diagonalizes the eigenvalue problem in the Fourier direction k with eigenvalues $\epsilon_\nu = \omega\nu$. It follows that

$$\begin{aligned}&k\omega A_{l,k} + \frac{\mu\epsilon_l}{2}(A_{l,k-1} + A_{l,k+1}) \\ &\quad = \sum_\nu c_{l,\nu} \Big[k\omega B^{(\nu)}_{l,k} + \frac{\mu\epsilon_l}{2}\big(B^{(\nu)}_{l,k-1} + B^{(\nu)}_{l,k+1}\big) \Big] \\ &\quad = \sum_\nu \omega\nu\, c_{l,\nu} B^{(\nu)}_{l,k}.\end{aligned} \tag{A8}$$

The eigenvalue problem Eq. (A6) in the new basis $\mathcal{B}$ reads

$$\begin{aligned}E \sum_\nu c_{l,\nu} B^{(\nu)}_{l,k} &= \sum_\nu \big[(\epsilon_l + \omega\nu) c_{l,\nu} B^{(\nu)}_{l,k} \\ &\quad - \lambda\big(\xi^-_{l,k} c_{l-1,\nu} B^{(\nu)}_{l-1,k} + \xi^+_{l,k} c_{l+1,\nu} B^{(\nu)}_{l+1,k}\big)\big].\end{aligned} \tag{A9}$$

We multiply both sides of Eq. (A9) with a second Bessel function $B^{(\nu_2)}_{l,k}$ of index ν_2 and then sum over k. Using the Bessel function orthonormality relation [22,23]

$$\sum_k B^{(\nu)}_{l,k} B^{(\nu_2)}_{l,k} = \sum_k J_{k-\nu}\left(\frac{\mu\epsilon_l}{\omega}\right) J_{k-\nu_2}\left(\frac{\mu\epsilon_l}{\omega}\right) = \delta_{\nu,\nu_2} \tag{A10}$$

in Eq. (A9), we obtain

$$\begin{aligned}E \sum_k \sum_\nu c_{l,\nu} B^{(\nu)}_{l,k} B^{(\nu_2)}_{l,k} &= E c_{l,\nu}, \\ \sum_k \sum_\nu (\epsilon_l + \omega\nu) c_{l,\nu} B^{(\nu)}_{l,k} B^{(\nu_2)}_{l,k} &= (\epsilon_l + \omega\nu) c_{l,\nu}.\end{aligned} \tag{A11}$$

The matrix elements (hopping) along the real direction l become

$$\sum_k \sum_\nu \xi^{\pm}_{l,k} c_{l\pm1,\nu} B^{(\nu)}_{l\pm1,k} B^{(\nu_2)}_{l,k} = \sum_\nu c_{l\pm1,\nu} \left(\sum_k \xi^{\pm}_{l,k} B^{(\nu)}_{l\pm1,k} B^{(\nu_2)}_{l,k} \right). \quad \text{(A12)}$$

Using Graf's generalization of Neumann's addition theorem [22,23]

$$\sum_k e^{ik\theta} J_{\nu+k}(x) J_k(y) = \left(\frac{x - ye^{-i\theta}}{x - ye^{i\theta}} \right)^{\frac{\nu}{2}} J_\nu(\sqrt{x^2 + y^2 - 2xy\cos\theta}) \quad \text{(A13)}$$

and defining the random phase difference

$$\theta^{\pm}_l = \phi_l - \phi_{l\pm1}, \quad \text{(A14)}$$

Eq. (A12) is modified as

$$\sum_k \sum_\nu \xi^{\pm}_{l,k} c_{l\pm1,\nu} B^{(\nu)}_{l\pm1,k} B^{(\nu_2)}_{l,k} = \sum_s (\sigma^{\pm}_l)^s J_s(\Delta^{\pm}_l) c_{l\pm1,\nu-s}, \quad \text{(A15)}$$

where

$$\sigma^{\pm}_l = \left(\frac{\epsilon_l - e^{-i\theta^{\pm}_l} \epsilon_{l\pm1}}{\epsilon_l - e^{i\theta^{\pm}_l} \epsilon_{l\pm1}} \right)^{\frac{1}{2}},$$
$$\Delta^{\pm}_l = \frac{\mu}{\omega} \sqrt{\epsilon_l^2 + \epsilon_{l\pm1}^2 - 2\epsilon_l \epsilon_{l\pm1} \cos\theta^{\pm}_l}. \quad \text{(A16)}$$

Since the complex coefficient $\sigma^{\pm}_l$ has absolute value equal to unity, we rewrite it as

$$\sigma^{\pm}_l = e^{i\varphi^{\pm}_l}, \quad \tan\varphi^{\pm}_l = -\frac{\epsilon_{l\pm1} \sin\theta^{\pm}_l}{\epsilon_l - \epsilon_{l\pm1}\cos\theta^{\pm}_l}. \quad \text{(A17)}$$

The final eigenvalue problem becomes [Eq. (10)]

$$E c_{l,\nu} = (\epsilon_l + \omega\nu) c_{l,\nu} - \lambda \sum_s [e^{is\varphi^-_l} J_s(\Delta^-_l) c_{l-1,\nu-s} + e^{is\varphi^+_l} J_s(\Delta^+_l) c_{l+1,\nu-s}]. \quad \text{(A18)}$$

[1] P. W. Anderson, Phys. Rev. **109**, 1492 (1958).
[2] E. Abrahams, P. W. Anderson, D. C. Licciardello, and T. V. Ramakrishnan, Phys. Rev. Lett. **42**, 673 (1979).
[3] B. R. Bulka, B. Kramer, and A. MacKinnon, Z. Phys. B **60**, 13 (1985).
[4] Y. Lahini, A. Avidan, F. Pozzi, M. Sorel, R. Morandotti, D. N. Christodoulides, and Y. Silberberg, Phys. Rev. Lett. **100**, 013906 (2008).
[5] J. Billy, V. Josse, Z. Zuo, A. Bernard, B. Hambrecht, P. Lugan, D. Clément, L. Sanchez-Palencia, P. Bouyer, and A. Aspect, Nature (London) **453**, 891 (2008).
[6] G. Roati, C. D'Errico, L. Fallani, M. Fattori, C. Fort, M. Zaccanti, G. Modugno, M. Modugno, and M. Inguscio, Nature (London) **453**, 895 (2008).
[7] K. Rayanov, G. Radons, and S. Flach, Phys. Rev. E **88**, 012901 (2013).
[8] T. Nakanishi, T. Ohtsuki, and T. Kawarabayashi, J. Phys. Soc. Jpn. **66**, 949 (1997).
[9] H. Yamada, K. S. Ikeda, and M. Goda, Phys. Lett. A **182**, 77 (1993).
[10] H. Yamada and K. S. Ikeda, Phys. Lett. A **248**, 179 (1998).
[11] H. Yamada and K. S. Ikeda, Phys. Rev. E **59**, 5214 (1999).
[12] D. F. Martinez and R. A. Molina, Phys. Rev. B **73**, 073104 (2006).
[13] Victor A. Gopar and Rafael A. Molina, Phys. Rev. B **81**, 195415 (2010).
[14] T. Kitagawa, T. Oka, and E. Demler, Ann. Phys. (NY) **327**, 1868 (2012).
[15] B. Kramer and A. MacKinnon, Rep. Prog. Phys. **56**, 1469 (1993).
[16] P. Windpassinger and K. Sengstock, Rep. Prog. Phys. **76**, 086401 (2013).
[17] I. Bloch, Nat. Phys. **1**, 23 (2005).
[18] G. Floquet, Ann. Sci. De l'ENS **12**, 2nd ed., 47 (1883).
[19] J. H. Shirley, Phys. Rev. **138**, B979 (1965).
[20] H. Fukuyama, R. A. Bari, and H. C. Fogedby, Phys. Rev. B **8**, 5579 (1973).
[21] D. O. Krimer, R. Khomeriki, and S. Flach, Phys. Rev. E **80**, 036201 (2009).
[22] G. N. Watson, *A Treatise on the Theory of Bessel Function* (Cambridge University Press, Cambridge, 1922).
[23] M. Abramowitz and I. A. Stegun, *Handbook of Mathematical Functions* (Dover, New York, 1972).
[24] O. N. Dorokhov, Solid State Commun. **46**, 605 (1983).
[25] P. A. Mello, P. Pereyra, and N. Kummar, Ann. Phys. (NY) **181**, 290 (1988).
[26] S. Kim, S. Ostlund, and G. Yu, Physica D **31**, 117 (1988).
[27] J. Laskar and P. Robutel, Celest. Mech. Dyn. Astron. **80**, 39 (2001).
[28] Ch. Skokos, E. Gerlach, J. D. Bodyfelt, G. Papamikos, and S. Eggl, Phys. Lett. A **378**, 1809 (2014); E. Gerlach, S. Eggl, Ch. Skokos, J. D. Bodyfelt, and G. Papamikos, arXiv:1306.0627v1; E. Gerlach, J. Meichsner, and Ch. Skokos, arXiv:1512.07778.
[29] A. Soffer and W. Wang, Commun. Part. Diff. Eq. **28**, 333 (2003).
[30] J. Bourgain and W. Wang, Commun. Math. Phys. **248**, 429 (2004).